

Article

Modified Transceiver Antenna for NQR Detection of Explosive Objects in Demining Conditions

Andrii Samila ¹, Oleksandra Hotra ^{2,*}, Oleksandr Moisiuk ¹, Mykola Khobzei ¹ and Taras Kazemirskiy ¹

¹ Department of Radio Engineering and Information Security, Yuriy Fedkovych Chernivtsi National University, Kotsyubynsky 2, 58002 Chernivtsi, Ukraine

² Department of Electronics and Information Technology, Lublin University of Technology, Nadbystrzycka 38D, 20-618 Lublin, Poland

* Correspondence: o.hotra@pollub.pl

Abstract: This paper presents the conceptual stages of the simulation and development of a modified transceiver antenna for a high-power pulsed nuclear quadrupole resonance (NQR) detector of explosives containing the ¹⁴N isotope. At a frequency of 4.645 MHz, better characteristics are obtained using a nine-turn coil shaped as half of a Fermat spiral with an outer radius of 75 mm. Using a COMSOL Multiphysics numerical parametric simulation and a materials browser, it was possible to calculate a physical system with parameters as close to reality as possible. According to the results of the experimental studies of the radio frequency (RF) energy, the proposed antenna features an increase in the working area compared to a similar antenna, the topology of the conductive coil of which has the form of an Archimedean spiral. The resulting diagrams of the distribution of the magnetic induction also indicate that the topology of the electromagnetic (EM) field does not depend on the orientation of the sample under study relative to the axis of the radial symmetry observed in square–rectangular planar antennas.

Keywords: nuclear quadrupole resonance; spiral antenna; Fermat spiral; magnetic field decay; simulation



Citation: Samila, A.; Hotra, O.;

Moisiuk, O.; Khobzei, M.;

Kazemirskiy, T. Modified Transceiver

Antenna for NQR Detection of

Explosive Objects in Demining

Conditions. *Energies* **2022**, *15*, 7348.

<https://doi.org/10.3390/en15197348>

Academic Editor: Andrea Mariscotti

Received: 3 September 2022

Accepted: 5 October 2022

Published: 6 October 2022

Publisher's Note: MDPI stays neutral with regard to jurisdictional claims in published maps and institutional affiliations.



Copyright: © 2022 by the authors. Licensee MDPI, Basel, Switzerland. This article is an open access article distributed under the terms and conditions of the Creative Commons Attribution (CC BY) license (<https://creativecommons.org/licenses/by/4.0/>).

1. Introduction

One of the key features of the development of our civilization is the protection of people's lives. However, recently, an increase in military conflicts and terrorist acts has occurred. Sometimes, such dangerous situations can be prevented by using novel equipment for detecting explosive objects [1–4].

Despite the intensive development of science and technology, EM metal detectors, the first prototypes of which were used during the Second World War, are still the main devices for detecting explosive objects. Metal detectors of this type have a number of disadvantages. Due to the fact that the EM signal reflected from the anti-personnel mine is much weaker, the sapper must increase the sensitivity of the detector. However, at higher sensitivities, many other metal objects, such as nails and hull debris, interfere with the detector. Unfortunately, the next step is the most difficult, since it is necessary to separate the signals of real explosive devices from “false alarms”. The sapper performs a very delicate extraction with a pointed stick to classify the source of the reflected signal, which could be a landmine, a forgery, or simply a rusty nail. In this sense, while the search for mines is quite simple, separating them from other objects is difficult and extremely dangerous [1]. Another significant disadvantage of EM metal detectors is their inability to detect explosive objects in non-metallic containers (hand luggage, envelopes, plastic containers, etc.) [2].

An alternative method for detecting explosives is the use of highly sensitive vapor sensors. However, the evaporation of explosives used in landmines is rather weak. Furthermore, modern mines are produced with a hermetically packed explosive in a polymer case. Since the vapors and particles of explosives are quite sticky, the infiltration of explosives

through the case and then through the soil is slow and inefficient. Studies have shown that under field conditions, even highly sensitive vapor sensors may not detect vapor plumes from mines [5].

A basis for the development of promising hardware and software tools for the detection of explosives is the idea of using the pulse NQR method to observe the free induction decay of the ^{14}N isotope [2,6–8]. Based on the analysis and with regard to the obvious advantages of the method (such as its non-destructive effect, the possibility of studying inhomogeneous mixtures, and rapid analysis without preliminary sample preparation), it was found that the development of hardware and software for detecting hazardous substances based on NQR is more appropriate than other methods [9,10].

This paper presents a simulation and an experimental prototype of a modified transceiver antenna with an extended working area for detecting explosive objects using the NQR method in demining conditions.

2. Methods of Geometric and Spatial Simulation of a Modified Antenna

2.1. Statement of the Research Problem

In most cases, the transceiver antenna of the NQR explosive detector is a spiral RF coil operating in the near EM field [11,12]. In order to adapt to the functional requirements of demining, the size of the coil is chosen in proportion to the size of explosive object. In the case of NQR observation, it is important to design the coil geometry with regard to the highest possible signal-to-noise ratio (SNR) of the detector. This scientific problem was considered in detail in [13]. The problem mostly depends on the noise level of the detector's receiving path and, above all, on the quality of the coil. To analytically estimate the SNR of NQR detectors operating in the HF and VHF frequency bands, we can apply the expression [14]:

$$\text{SNR} = \frac{1}{8} \cdot \left(\frac{\omega^3 \cdot \eta \cdot Q \cdot V_S}{2 \cdot \mu_0 \cdot k \cdot T \cdot N_F \cdot \Delta F} \cdot \frac{T_2}{T_1} \right)^{1/2} \cdot \frac{\chi_0}{\gamma} \quad (1)$$

where η is the energy-transfer coefficient, Q is the quality factor, V_S is the volume of the sample, T_1 and T_2 are the relaxation-time constants, μ_0 is the permeability, k is the Boltzmann constant, T is the absolute temperature, N_F is the noise figure for the detector's receiving path preamplifier, ΔF is the detector's receiving-path bandwidth, χ_0 is the magnetic susceptibility, ω is the angular frequency of the resonance, and γ is the gyromagnetic ratio.

The parameter η is defined as the ratio of magnetic energy stored in the sample to magnetic energy stored in the antenna [14]. It also depends on the homogeneity of magnetic induction (no more than 15%). This is especially important when using the pulse method for detecting resonant signals, where the maximum level of the free-induction decay signal largely depends on the magnetic induction in the antenna during excitation [15].

Improving the homogeneity of the EM field is especially important for detecting low-level responses from substances containing nitrogen atoms (^{14}N). Therefore, when choosing the configuration of the coil and the approach to its manufacture, the quality parameter ηQ , taking into account the homogeneity of the EM field, is crucial.

2.2. Substantiation of Geometry and Development of the Spiral-Coil Model in Comsol Multiphysics

To simulate three-dimensional fields, the finite-element method has several applications [16–18]. The EM field distribution near the proposed NQR detector antenna was calculated using the analytical capabilities of COMSOL Multiphysics software, which offers wide functionality for the implementation and study of models of physical fields [19].

To improve the EM field distribution in the working area of the antenna, it is necessary to decrease the distance between the turns of the flat coil with increase in distance from its geometric center. The conclusion about the reduction in the interturn distance is made on the basis of an analogy with respect to the law of inverted squares. The solution of this problem is possible by using the Fermat spiral expression to construct the coil geometry.

Fermat spiral is a type of Archimedean spiral [20]. However, it differs from the usual Archimedean spiral in that the distance between adjacent turns in the former spiral is always the same, and this pattern is not preserved in Fermat spiral. General view of the equation of a plane curve in polar coordinates is as follows:

$$r^2 = a^2\theta \quad (2)$$

where r is the radial coordinate, a is the angle of polar inclination between the tangent to the curve and the corresponding polar circle, and θ is the azimuth.

Since for any given positive value of θ there are two values of r equal in modulus but opposite in sign

$$r = \pm a\theta^{1/2} \quad (3)$$

to calculate the geometry of the required coil shaped as half of Fermat spiral, we take into account a special case for $r > 0$.

The equations described above, converted from the polar to Cartesian coordinates, were adapted to synthesize a numerical model of the coil geometry in COMSOL Multiphysics.

To adapt to the functional requirements of demining, the size of the coil was chosen to be proportional to the size of the anti-personnel mine, resulting in a coil diameter of 150 mm. The number of turns was chosen according to the results of magnetic-field simulations; nine turns showed the best result for the given coil sizes. A spiral thickness of 3 mm was chosen, taking into account that the maximum current in the coil did not exceed 1.5 A. Other parameters were calculated according to the equations given in Table 1.

Table 1. System of equations and parameters for simulation of coil geometry in COMSOL Multiphysics.

| Description | Name | Expression | Value |
|-------------------------|----------|--------------------------------------|-------------|
| Initial spiral radius | a1 | 9 | 9 mm |
| Final spiral radius | Af | 75 | 75 mm |
| Spiral growth rate | b1 | $(af - a1)/(2 \times \pi \times n1)$ | 1.1671 r.u. |
| Updated growth rate | b2 | $(gap + thick)/(2 \times \pi)$ | 1.1671 r.u. |
| Turn-to-turn distance | Distance | $(af - a1)/n1$ | 7.3333 r.u. |
| Gap distance | Gap | distance-thick | 4.3333 r.u. |
| Number of turns | n1 | 9 | 9 |
| Initial angle | Theta_0 | 0 | 0 deg |
| Final angle | Theta_f | $(af - a1)/b1$ | 56.549 deg |
| Thickness of the spiral | Thick | 3 | 3 mm |

For simulation by the finite-element method, a technique was used, which was considered in detail in [21]. The geometric model (calculation area) of the proposed antenna, obtained on the basis of its numerical model, is shown in Figure 1. Structurally, the antenna is a flat coil in the form of a parabolic spiral with the following parameters: outer radius, number of turns, winding pitch, geometry and material of conductive conductors, etc. This data, as well as information about the initial simulation conditions, are global top-level definitions in Model Builder. The geometry of the coil is represented by half of a Fermat spiral with a relative tolerance of 10^{-5} , which is technologically easy to produce on a glass-fiber-epoxy printed-circuit-board laminate. We used FR-4-35/0-1.5 mm (at a frequency of 1 MHz, the typical dielectric constant is 4.5 and the dielectric loss angle tangent is 0.017) with a one-sided metal-coating 35 μm thick. At the ends of the flat coil, there are parallel rectangular contact pads, which serve to connect the lumped port (LP) excitation source with a characteristic impedance of 50 ohms and the capacitor of the parallel oscillatory circuit of the NQR detector input circle — lumped element (LE) (Figure 1). Copper with electrical conductivity 5.998×10^{-7} S/m and relative magnetic permeability 0.99999 was chosen as the material of conductive elements. A fixed capacitor was used to simplify the simulation. In the real experiment, a variable capacitor was used to fine-tune the input circuit of the NQR detector to the resonance frequency.

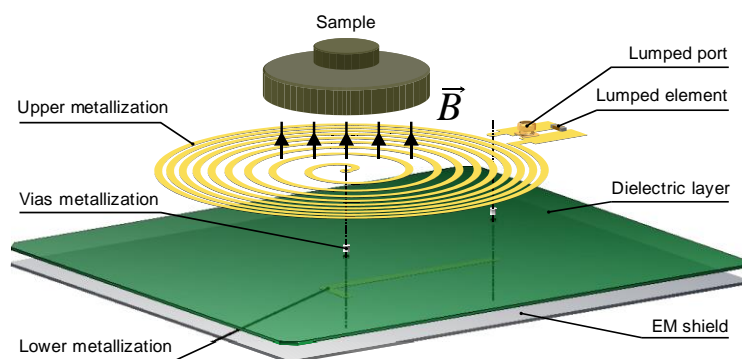


Figure 1. Geometric model of a spiral coil. General view with excitation port and resonant circuit capacitor.

The bottom metal plate is the electromagnetic shield. In the experimental model, a steel sheet with dimensions of 220 mm × 190 mm and a thickness of 1 mm was used. In the future layout, the bottom of the metal case of the NQR detector antenna will serve as the shield.

In order to simulate perfect conditions for the absorption of electromagnetic radiation energy and prevent erroneous reflections, the geometrical model of the antenna is limited to an air cube with the following parameters: side equal to 400 mm, electrical conductivity equal to 0 S/m, relative magnetic permeability equal to 1, temperature equal to 293.15 K and pressure equal to 1 atm.

Numerical simulation was carried out using the *AC/DC* and *RF* modules of the program [19]. Specifically, the calculation of the EM topology of the magnetic field was performed using the parameterized interfaces *Magnetic Fields (mf)* and *Electric Currents in Shells (ecis)*. The response of the model, which is subjected to harmonic excitation in the operating-frequency range, was calculated using the parameterized interface *Electromagnetic Waves, Frequency Domain (emw)*, and adaptive frequency scanning for more accurate frequency resolution. Wave Equation (4) describes the region of an air cube and the region of copper conductive elements:

$$\nabla \times \mu_r^{-1}(\nabla \times E) - k_0^2 \left(E_r - \frac{j\sigma}{\omega E_0} \right) E = 0 \quad (4)$$

For the electrical connection of LP and LE with the end terminals of the coil, lossless metal conductors were added, represented in the simulation stage of the boundary condition (5) of the perfect electrical conductor (PEC). Thus, the requirements for computing resources were significantly reduced:

$$n \times E = 0 \quad (5)$$

At the previous simulation stage, parameterized interfaces were adjusted and mesh sensitivity was analyzed (Figure 2).

The mesh step (Figure 3) was chosen as optimal, taking into account the fact that its increase leads to deterioration in the simulation accuracy, but its reduction leads to errors in fractional operations. Furthermore, reducing the mesh step requires a significant amount of hardware-computing resources. The optimal mesh parameters were established empirically: the largest element size equal to 200 mm, the smallest element size equal to 0.6 mm, the largest increment of the element size equal to 1.35 mm, the curvature factor equal to 0.3, and the narrow area resolution equal to 0.85. These values were determined for the model under study in order to improve the simulation efficiency. The appearance of the parametric mesh superimposed on the geometric model of the spiral coil is shown in Figure 3a and an enlarged view of the mesh is shown in Figure 3b.

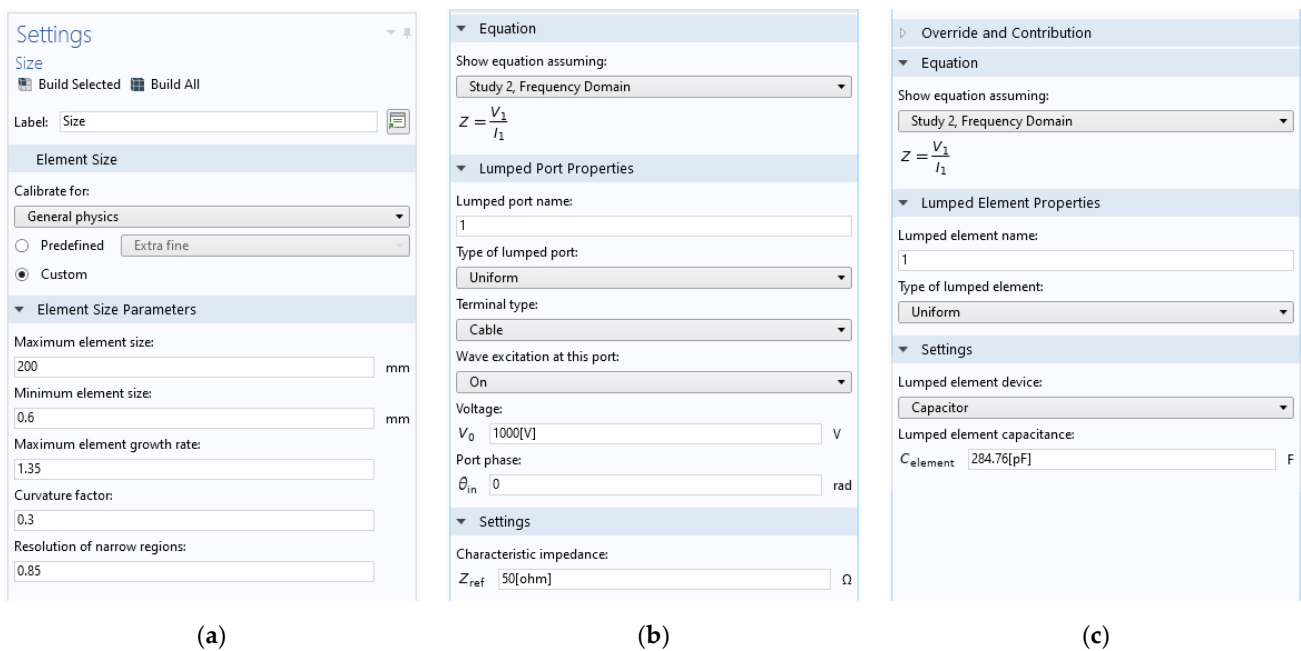


Figure 2. Configuring COMSOL interfaces: (a) Mesh; (b) lumped port; (c) lumped element.

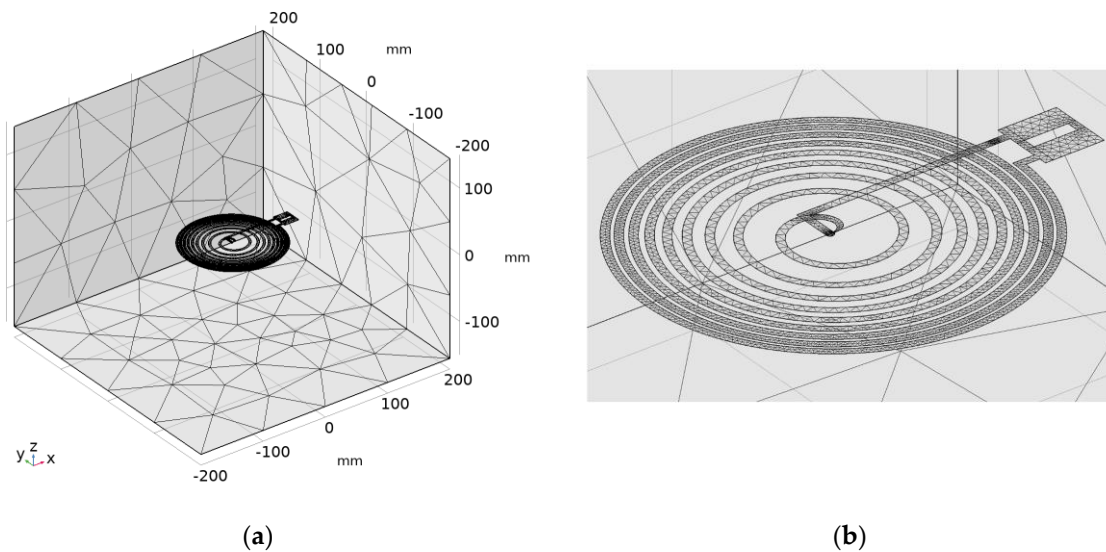


Figure 3. The finite-element mesh synthesized as a result of triangulation of the geometric model: (a) placement in the air cube, (b) detailed view of the antenna.

3. Discussion of Results

3.1. Analysis of Simulation Results

The simulation was performed on a workstation containing a HexaCore Intel Core i7-8700K microprocessor clocked at 4.3 GHz and 32 GB of DDR4 RAM. In order to compare the characteristics of the proposed antenna shaped as half of a Fermat spiral with an alternative classical Archimedean-spiral design, COMSOL Multiphysics also synthesized a numerical model of the geometry of the latter coil and tested both models using the parameterized *mf*, *ecis*, and *emw* interfaces. The electrical characteristics of the elements used in the study of the numerical models Fermat spiral coil and Archimedean spiral coil are given in Table 2.

Table 2. Electrical characteristics of elements used in the study of numerical models of Fermat spiral coil and Archimedean spiral coil.

| | Fermat Spiral Coil | Archimedean Spiral Coil |
|--|-------------------------------|-------------------------------|
| Coil inductance | $L = 8.386 \text{ uH}$ | $L = 4.955 \text{ uH}$ |
| Lumped element capacitance | $C = 140 \text{ pF}$ | $C = 237 \text{ pF}$ |
| Frequency | $F = 4.645 \text{ MHz}$ | $F = 4.645 \text{ MHz}$ |
| Characteristic impedance of resonant circuit | $\rho = 244.745 \text{ ohms}$ | $\rho = 144.593 \text{ ohms}$ |
| Coil resistance | $R = 0.15983 \text{ ohms}$ | $R = 0.15983 \text{ ohms}$ |
| Quality factor of resonant circuit | $Q = 1531$ | $Q = 905$ |

The simulation was carried out around the ^{14}N NQR frequency (4.645 MHz) in NaNO_2 [22]. This quadrupole core can serve as a kind of sensitivity marker for the NQR sensor of explosive objects, since it provides a weak signal of the free-induction-decay response, which was confirmed by our previous experimental studies. In order to investigate the frequency dependence of the impedance of a parallel oscillatory circuit with a resonance frequency of 4.645 MHz using the parametric simulation method, a capacitive lumped element was connected in parallel with the lumped port, the capacitance of which was determined individually for each coil from the following equation [23]:

$$C_t = \frac{r}{\sqrt{r\omega^2 Z_0(L^2\omega^2 + r^2 - rZ_0)}} \quad (6)$$

where L is the antenna inductance, ω is the angular frequency of the resonance, Z_0 is the input resistance of the NQR detector, and r is the active resistance of the antenna.

In order to find resonant modes for two coils with different geometries at frequencies of 4.4–4.9 MHz, the study was begun with a resolution of 0.1 MHz. The lumped capacitive element placed parallel to the lumped port was used for tuning. More accurate resonant modes were found using frequency-swing control algorithms in steps of 5 kHz.

The processing of the results of the numerical simulation was carried out by the built-in COMSOL tools using the “Results” menu.

From the data obtained using the numerical simulation, multilayer models of the EM field isosurface were built in the vicinity of the conductive elements of the investigated coils (Figures 4 and 5) [24]. The simulation took into account the limiting conditions that described the distribution of the EM field within the computational domain. In particular, Figure 5 shows the simulation results of the EM field at a frequency of 4.645 MHz for half of a Fermat spiral coil. It was established that for the modified coil (Figure 5) there was a larger area with increased uniformity of the EM field distribution than for the coil shaped as an Archimedean spiral (Figure 4). Moreover, for a more detailed study of the dimensions of the working area with a magnetic-induction inhomogeneity of no more than 15%, it was necessary to conduct an additional analysis of the results of the numerical simulation for individual sections of the computational domain.

In the study of both coils by numerical simulation, the dependences of the magnetic induction on the displacements along the radius vectors drawn parallel to the y -axis at distances of 20 mm and 40 mm from the XY plane were obtained (Figure 6). The analysis of these dependencies allows us to estimate the magnitude of the decrease in the intensity of the EM field radiation with increasing distance from the geometric center of the coils. It also explains how to place the sample under study. The dependences of the magnetic-induction distribution show that the zones of sufficient field homogeneity (10–15%) on both sides of the geometric center of the Archimedean spiral were ± 18 mm and ± 22 mm at distances from the XY plane of 20 mm and 40 mm, respectively, and, for the Fermat spiral of about 25 mm for the two cases. With the subsequent removal of the virtual sensor along the z axis for the modified coil, in contrast to the Archimedean spiral, there was no significant change in the radial dependence of the normalized magnetic induction.

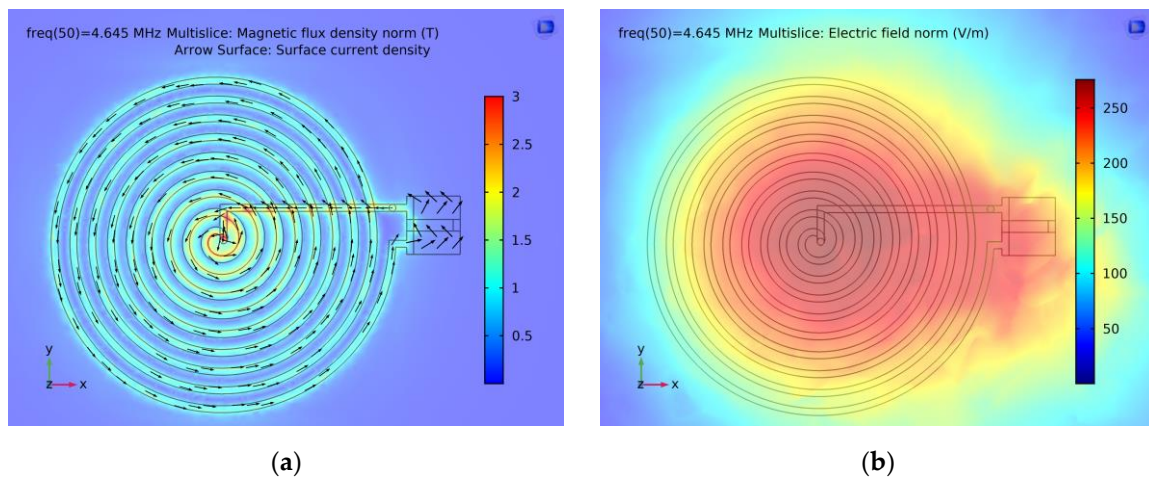


Figure 4. Visualization of the results of simulation of the EM field in the vicinity of the conductive elements of the NQR-detector-antenna model shaped as Archimedean spiral at a frequency of 4.645 MHz: (a) magnetic-field induction, (b) electric-field strength.

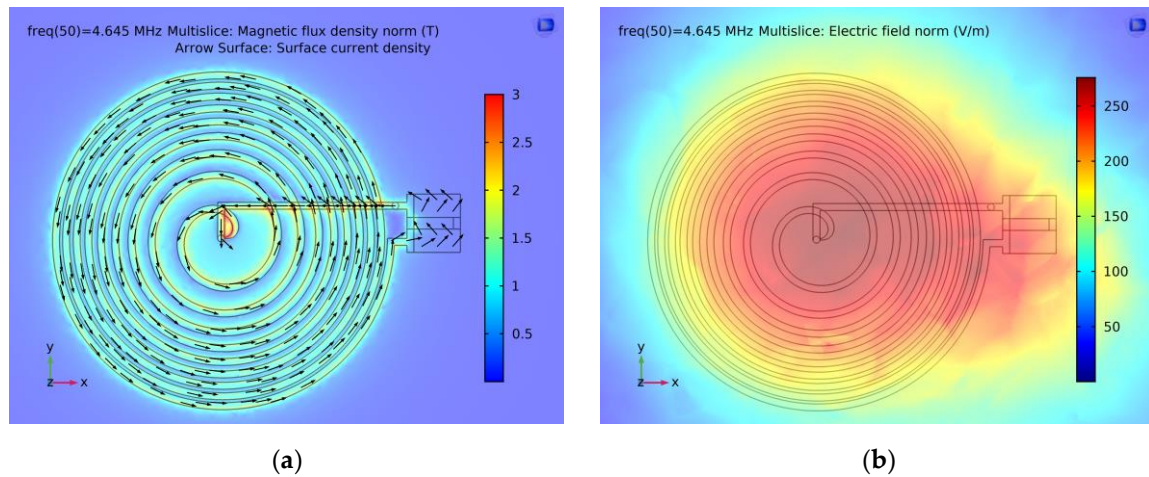


Figure 5. Visualization of the results of simulation of the EM field in the vicinity of the conductive elements of the model of the modified NQR detector antenna at a frequency of 4.645 MHz: (a) magnetic field induction, (b) electric-field strength.

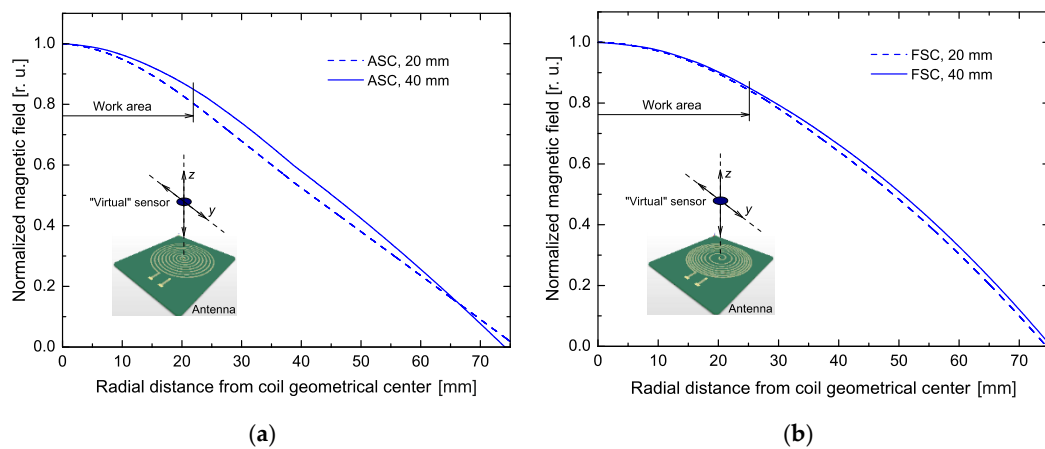


Figure 6. Simulation of magnetic-field decay at the frequency 4.645 MHz: (a) at distances of 20 mm and 40 mm from the Archimedean spiral coil; (b) at distances of 20 mm and 40 mm from the Fermat spiral coil. Working areas are shown at distance of 40 mm.

As noted above, the inhomogeneity of the magnetic induction is not the only parameter that must be considered. Considering the expression for H_1 in [25], we can see that to obtain the maximum EM field strength in the area of the sample, it is necessary to minimize the volume of the coil, while, at the same time, the quality factor should be maximized in the signal-reception mode. In order to determine the quality factor of the coils and their subsequent coordination with the transmitting and receiving equipment, an additional analysis of the frequency dependences of the impedance of the elements of the oscillatory circuits used in the study of the numerical models was carried out (Table 3).

Table 3. The results of analysis of the frequency dependences of the impedance of the elements of oscillatory circuits used in the study of the numerical models of Fermat spiral coil and Archimedean spiral coil.

| Frequency, MHz | Archimedean Spiral Coil | | | Fermat Spiral Coil | | |
|----------------|----------------------------------|-----------------------------------|----------------------------------|----------------------------------|-----------------------------------|----------------------------------|
| | Inductive Reactance X_L , ohms | Capacitive Reactance X_C , ohms | Full Impedance $ Z_{LC} $, ohms | Inductive Reactance X_L , ohms | Capacitive Reactance X_C , ohms | Full Impedance $ Z_{LC} $, ohms |
| 4.6100 | 143.52 | -145.67i | 9741.1 | 242.86 | -246.60i | 16,035 |
| 4.6150 | 143.68 | -145.51i | 11,407 | 243.13 | -246.33i | 18,689 |
| 4.6200 | 143.84 | -145.35i | 13,758 | 243.39 | -246.07i | 22,393 |
| 4.6250 | 143.99 | -145.20i | 17,324 | 243.65 | -245.80i | 27,920 |
| 4.6300 | 144.15 | -145.04i | 23,377 | 243.92 | -245.53i | 37,057 |
| 4.6350 | 144.30 | -144.88i | 35,908 | 244.18 | -245.27i | 55,051 |
| 4.6400 | 144.46 | -144.73i | 77,307 | 244.44 | -245.00i | 1.0691×10^5 |
| 4.6450 | 144.61 | -144.57i | 5.0980×10^5 | 244.71 | -244.74i | 1.8131×10^6 |
| 4.6500 | 144.77 | -144.42i | 59,373 | 244.97 | -244.48i | 1.2135×10^5 |
| 4.6550 | 144.92 | -144.26i | 31,538 | 245.23 | -244.22i | 58,741 |
| 4.6600 | 145.08 | -144.11i | 21,479 | 245.50 | -243.95i | 38,764 |
| 4.6650 | 145.24 | -143.95i | 16,289 | 245.76 | -243.69i | 28,934 |
| 4.6700 | 145.39 | -143.80i | 13,122 | 246.02 | -243.43i | 23,086 |
| 4.6750 | 145.55 | -143.64i | 10,988 | 246.29 | -243.17i | 19,208 |
| 4.6800 | 145.70 | -143.49i | 9452.2 | 246.55 | -242.91i | 16,448 |

The results obtained by simulating the frequency dependences of the lumped-port impedance for both coils in the frequency range 4.55–4.75 MHz are shown in Figure 7. Due to the near-doubling of the inductance (8.386 μ H vs. 4.955 μ H) and approximately the same active resistance, the quality factor of the modified coil increased by approximately 69%, which allowed us to improve the optimal conditions for receiving NQR signals.

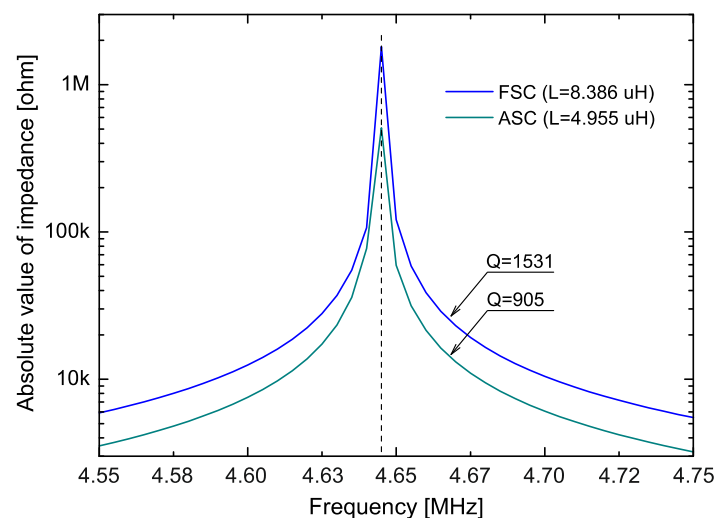


Figure 7. Simulating the frequency dependences of the lumped-port impedance in the frequency range 4.55–4.75 MHz.

3.2. Experimental Studies

Based on the results obtained using the computer simulations, experimental models of two transceiver antennas were constructed. These were structurally identical to the geometric models developed in the COMSOL Multiphysics program. The models were fabricated by chemical etching on FR-4-35/0–1.5-millimeter glass-fiber-epoxy laminate. Figure 8 shows photographs of the experimental layouts of the antennas, which were further investigated to verify the topology of the magnetic induction. The diameters of both spirals were 150 mm, with a conductor width of 3 mm, the distance between the centers of the turns of the Archimedean spiral antenna (Figure 8a) was 8.45 mm. The distance between the centers of the turns of the modified antenna (Figure 8b) was determined based on the numerical model of the coil geometry shaped as half of a Fermat spiral.

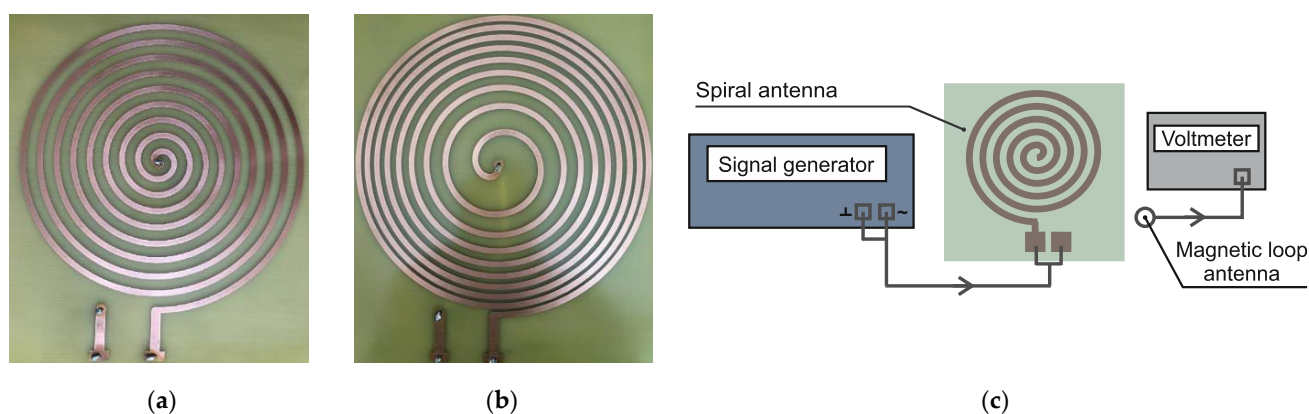


Figure 8. Experimental studies: (a) model of the antenna in the form of an Archimedean spiral; (b) layout of the modified antenna; (c) equivalent scheme of the experimental setup.

An equivalent scheme of the experimental setup for studying the topology of the magnetic induction is shown in Figure 8c. It consisted of a spiral antenna, an RF signal generator, and a voltmeter with a magnetic-loop antenna connected via an SMA connector, which acted as a scanning device of the EM field. Since the magnetic-loop antenna was in the zone of close-field interaction with the antenna under study, it was possible to detect the value of the electric current in the circuit of the latter, which was proportional to the magnetic induction in accordance with the Biot–Savart–Laplace law. To prevent a short circuit in the coil circuit, a resistor with a nominal resistance of 1 kohm was connected in series between the generator and the antenna under study.

To measure the topology of the field distribution, a two-coordinate device was used, which made it possible to move the magnetic-loop antenna with a step of 1 mm along two mutually perpendicular axes to control the longitudinal (B_X) and transverse (B_Y) components of the magnetic induction. The experimental studies were performed at a frequency of 4.645 MHz by scanning the field at distances of 20 mm and 40 mm from the surfaces of the studied antennas with a step of 5 mm along the spirals, and 10 mm outside them. The remaining experimental conditions were identical to those of the computer simulation.

Figure 9 shows the results of the experimental studies in the form of the relative distributions of the magnetic induction $B_1(y)/B_1(0)$ for two antenna variants. In the case of a modified antenna, there was a more uniform distribution of magnetic induction along the radius of the spiral than in that of the Archimedean spiral, where the maximum values of the magnetic induction were localized in the center. Therefore, the zones of permissible field inhomogeneity on both sides of the geometric center of the antenna in the form of the Archimedean spiral were: ± 14 mm and ± 18 mm at distances from the XY plane of 20 mm and 40 mm, respectively. For the modified antenna, the figures were approximately ± 29 mm for the two cases. As in the case of the computer simulation, further removal of the loop antenna from the modified coil along the z axis did not lead to a significant

change in the radial dependence of the normalized magnetic induction. Therefore, for the proposed coil, in addition to increasing the working area, the dimension of this area does not significantly depend on the distance of the test sample (Table 4).

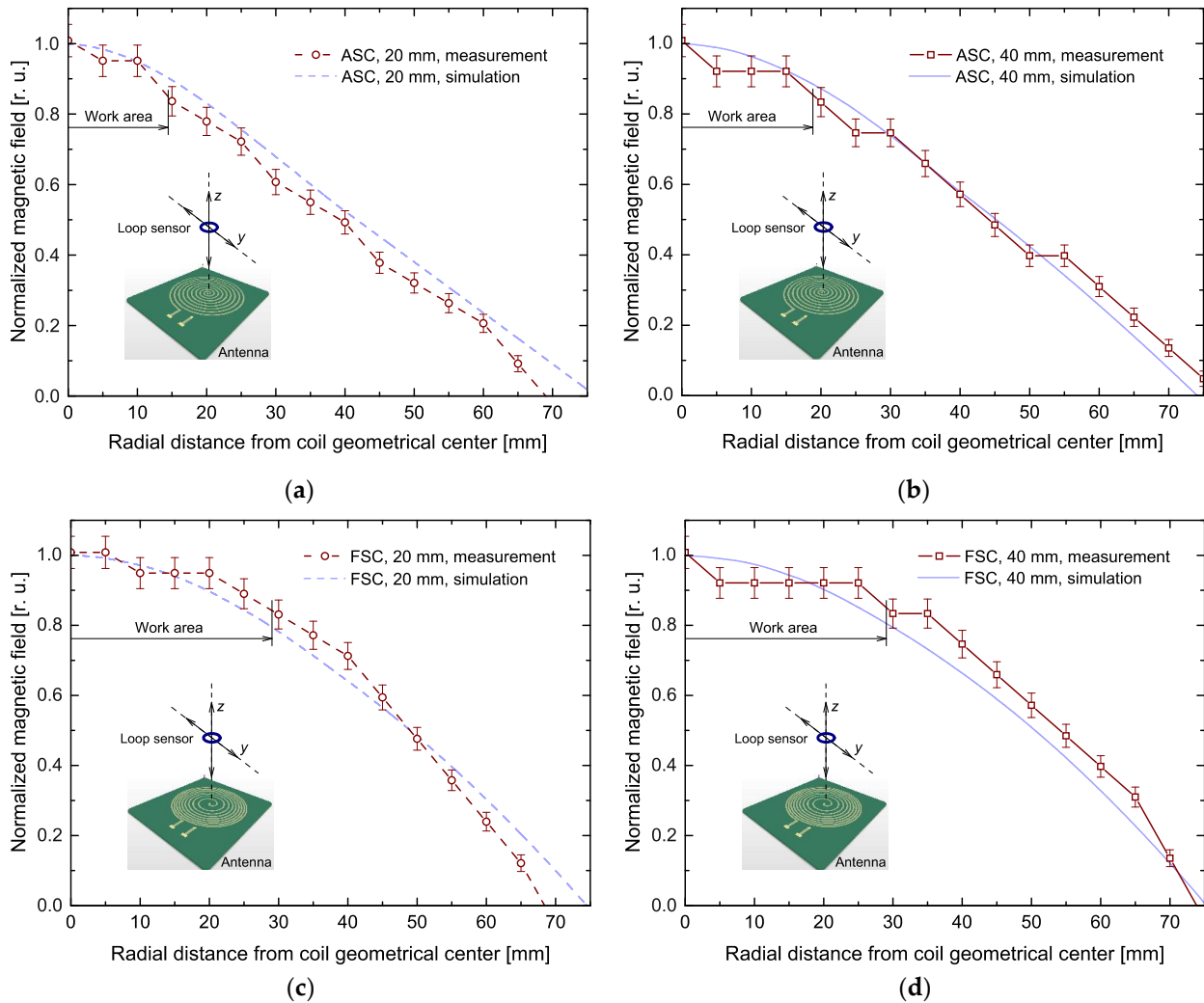


Figure 9. Comparison of experimental and simulation results of magnetic-field decay at the frequency 4.645 MHz: (a) at a distance of 20 mm from the Archimedean spiral coil; (b) at a distance of 40 mm from the Archimedean spiral coil; (c) at a distance of 20 mm from the Fermat spiral coil; (d) at a distance of 40 mm from the Fermat spiral coil.

Table 4. Comparison of the working areas of the investigated coils.

| Investigation Type | Working Area of the Archimedean Spiral Coil | Working Area of the Fermat Spiral Coil | Ratio | Increase |
|------------------------------|---|--|-------|----------|
| Simulation, distance 20 mm | 36 mm | 50 mm | 1.39 | 14 mm |
| Simulation, distance 40 mm | 44 mm | 50 mm | 1.14 | 6 mm |
| Experimental, distance 20 mm | 24 mm | 58 mm | 2.42 | 34 mm |
| Experimental, distance 40 mm | 36 mm | 58 mm | 1.61 | 22 mm |

4. Conclusions

According to the results of the analysis, the complex task of detection by the pulsed NQR method of weak signals of free-induction decay from the atoms contained in the vast majority of explosive substances (isotopes ^{14}N , ^{35}Cl , ^{37}Cl) requires the solution of a number of problems, which, in particular, involve optimizing the design of the detector's transceiver antenna. Summarizing the presented results, it is necessary to highlight the most important:

1. A numerical model of the coil geometry was synthesized in COMSOL Multiphysics, which allowed the expansion of the working area compared to the classical version of the spiral coil. This was achieved by compensating for the weakening of the magnetic induction at the edges of the coil.
2. The zones of sufficient field homogeneity (10–15%) on both sides of the geometric center of the coil shaped as half of a Fermat spiral were studied. It was established that the zones of permissible field inhomogeneity on both sides of the geometric center of the antenna in the form of the Archimedean spiral were ± 14 mm and ± 18 mm, at distances of 20 mm and 40 mm from its surface, respectively. For the modified antenna, these values were approximately ± 29 mm for the two locations of the measuring sensor.
3. The obtained magnetic-induction-distribution diagrams also showed that the volume of the working area did not significantly depend on the distance of the object of study, and the topology of the EM field did not depend on the orientation of the sample relative to the radial-symmetry axis observed in the planar antennas.
4. The results obtained by simulating the frequency dependences of the lumped-port impedance indicate that, the near-doubling of the inductance, the quality factor of the modified coil increased from 905 to 1531, which contributed to an increase in the sensitivity of the input circuit of the radio-receiving path of the detector in the NQR signal-reception mode.

In general, the research confirmed that the obtained parameters of the proposed transceiver antenna meet the conditions of the task and allow its effective use in the development of portable, pulsed NQR detectors of explosives. In addition, the proposed antenna can also be used in medium-power wireless power-transmission systems.

Author Contributions: Conceptualization, A.S. and O.H.; methodology, A.S. and O.M.; validation, O.H. and A.S.; formal analysis, A.S. and O.M.; investigation, O.M., M.K. and T.K.; resources, O.M., M.K. and T.K.; writing—original draft preparation, O.M., M.K. and T.K.; writing—review and editing, O.H. and A.S.; visualization, O.H.; supervision, A.S. and O.H. All authors have read and agreed to the published version of the manuscript.

Funding: This research was supported by the Lublin University of Technology, grant number: FD-20/EE-2/306.

Data Availability Statement: Not applicable.

Conflicts of Interest: The authors declare no conflict of interest.

References

1. September 2001 Test Results of an Acoustic Instrumented Prodder. Available online: <https://www.gichd.org/fileadmin/GICHD-resources/rec-documents/Russell.37-2.pdf> (accessed on 18 June 2022).
2. Apih, T.; Rameev, B.; Mozzhukhin, G.; Barras, J. Magnetic resonance detection of explosives and illicit materials. In *NATO Science for Peace and Security Series B: Physics and Biophysics*; Springer: Dordrecht, The Netherlands, 2014.
3. Khusnutdinov, R.R.; Mozzhukhin, G.V.; Konov, A.B. Two-frequency planar gradiometer for distant NQR detection of explosives. *Appl. Magn. Reson.* **2021**, *52*, 1787–1797. [CrossRef]
4. Monea, C.; Iana, G.V.; Ionita, S.; Ionescu, L.M.; Zaharia, S.A.; Ilie, S.; Bizon, N. An optimized NQR spectrometer for detection of prohibited substances. *Measurement* **2020**, *151*, 107158. [CrossRef]
5. Gasser, R.; Thomas, T.H. Prodding to detect mines: A technique with a future. In Proceedings of the Second International Conference on the Detection of Abandoned Land Mines, Edinburgh, UK, 12–14 October 1998.

6. Samila, A.; Haliuk, S.; Krulikovskiy, O. Structural and functional synthesis of the radioelectronic means of a pulsed NQR. In Proceedings of the 15th International Conference DAS, Suceava, Romania, 2–4 July 2020.
7. Sorte, E.G. *Aerial Crosspolarized NQR-NMR: Buried Explosive Detection From a Safe Distance*; Technical Report; Sandia National Lab.: Albuquerque, NM, USA, 2020. [[CrossRef](#)]
8. Otagaki, Y.; Barras, J.; Kosmas, P. Improving detection of a portable NQR system for humanitarian demining using machine learning. *IEEE Trans. Geosci. Remote Sens.* **2022**, *60*, 1–11. [[CrossRef](#)]
9. Samila, A.; Hotra, O.; Majewski, J. Implementation of the configuration structure of an integrated computational core of a pulsed NQR sensor based on FPGA. *Sensors* **2021**, *21*, 6029. [[CrossRef](#)] [[PubMed](#)]
10. Samila, A.P.; Politsansky, L.F.; Hotra, O.Z. A portable digital multipulse NQR spectrometer for the study of the sensory properties, structure and defects in layered semiconductors. In Proceedings of the International Conference TCSET 2020, Lviv-Slavske, Ukraine, 25–29 February 2020.
11. Fenglong, H.; Gengguang, X.; Xueyi, H. Study of RF coil in NQR explosive detection system. *Procedia Eng.* **2012**, *43*, 302–306. [[CrossRef](#)]
12. Hemnani, P.; Rajarajan, A.K.; Joshi, G.; Ravindranath, S.V.G. Design of probe for NQR/NMR detection. *Int. J. Electr. Comput. Eng.* **2020**, *10*, 3468–3475. [[CrossRef](#)]
13. Samila, A. Simulation of magnetic field topology in a saddle-shaped coil of nuclear quadrupole resonance spectrometer. *Prog. Electromagn. Res. Lett.* **2015**, *56*, 67–73. [[CrossRef](#)]
14. Schneider, H.; Dullenkopf, P. Slotted tube resonator: A new NMR probe head at high observing frequencies. *Rev. Sci. Instrum.* **1977**, *48*, 68–73. [[CrossRef](#)]
15. Grechishkin, V.S.; Sinyavskii, N.Y. Remote nuclear quadrupole resonance in solids. *Phys. Usp.* **1993**, *36*, 980–1003. [[CrossRef](#)]
16. Rodríguez, J.M.; Carbonell, J.M.; Jonsén, P. Numerical methods for the modelling of chip formation. *Arch. Computat. Methods Eng.* **2020**, *27*, 387–412. [[CrossRef](#)]
17. Vovchuk, D.; Khobzei, M.; Filonov, D. Naked eye direction of arrival estimation with a Fresnel lens. *Sci. Rep.* **2022**, *12*, 2479. [[CrossRef](#)] [[PubMed](#)]
18. Glukhenkyi, O.I.; Goryslavets, Y.M.; Tokarevskiy, A.V. Three-dimensional simulation of single-phase electromagnetic stirrer of liquid metal. *Tech. Electrodyn.* **2013**, *5*, 77–84.
19. Understand, Predict, and Optimize Real-World Designs, Devices, and Processes with Simulation. Available online: <https://www.comsol.com/comsol-multiphysics> (accessed on 18 June 2022).
20. Hussain, I.; Woo, D.K. Self-inductance calculation of the Archimedean spiral coil. *Energies* **2022**, *15*, 253. [[CrossRef](#)]
21. Farantatos, P.; Barras, J.; Poplett, I.; Kosmas, P. Electromagnetic design of a spiral surface RF-coil transceiver for NQR-based explosive detection in the humanitarian demining setting. In Proceedings of the 2018 COMSOL Conference in Lausanne, Lausanne, Switzerland, 22–24 October 2018.
22. Jover, J.; Aissani, S.; Guendouz, L.; Thomas, A.; Canet, D. NQR detection of sodium nitrite recrystallized in wood. In *NATO Science for Peace and Security Series B: Physics and Biophysics*; Springer: Dordrecht, The Netherlands, 2014.
23. Majewski, A.; Walker, M. Design of Impedance Matching Networks for NMR and NQR Studies in the HF Band. Available online: <http://www.phys.ufl.edu/~majewski/letters/match.pdf> (accessed on 1 June 2022).
24. Moisiuk, O.; Samila, A. Features of using the Comsol Multiphysics software for modeling a spiral antenna of an NQR detector. In Proceedings of the International Conference TCSET 2022, Lviv-Slavske, Ukraine, 22–26 February 2022.
25. Hotra, O.; Samila, A. A low-cost digital pulsed coherent spectrometer for investigation of NQR in layered semiconductor GaSe and InSe crystals. *Electronics* **2020**, *9*, 1996. [[CrossRef](#)]